SLAC–PUB–6094
UCSB–HEP–93–02
March 1993
(T/E)

Evidence For Spin-One Resonance Production in the Reaction $\gamma\gamma^* \to \pi^+\pi^-\pi^0\pi^{0*}$

TPC/Two-Gamma Collaboration

D.A. Bauer,[g] R. Belcinski,[j] R.C. Berg,[d] H.H. Bingham,[a] C.D. Buchanan,[d]
D.O. Caldwell,[g] S-B. Chun,[d] A.R. Clark,[h] O.I. Dahl,[h] M. Daoudi,[e]
J.J. Eastman,[h] A.M. Eisner,[c] K.H. Fairfield,[l] G. Godfrey,[l] G.S. Greenbaum,[f]
J.M. Hauptman,[i] W. Hofmann,[k] R.L. Holtzapple,[l] S. Khacheryan,[d] K.T. Knöpfle,[k]
R.R. Kofler,[j] D.J. Lambert,[h] J.G. Layter,[e] W.T. Lin,[e] S.C. Loken,[h]
A. Lu,[g] G.R. Lynch,[h] J.E. Lys,[a] R.J. Madaras,[h] G.E. Masek,[f]
E.S. Miller,[f] N.A. Nicol,[h] D.R. Nygren,[h] J.Y. Oyang,[d] H.P. Paar,[f]
A.P.T. Palounek,[h] D.E. Pellett,[b] M.T. Ronan,[h] R.R. Ross,[h] G. Shapiro,[h]
B.C. Shen,[e] R.W. Stephens,[g†] M.L. Stevenson,[h] M.G. Strauss,[j] M.K. Sullivan,[c]
W. Vernon,[f] E.M. Wang,[h] Y-X. Wang,[c] W.A. Wenzel,[h] H. Yamamoto,[d]
S.J. Yellin,[g] G.P. Yost,[a] G. Zapalac,[l] and C. Zeitlin[b]

[a] *University of California, Berkeley, California 94720*
[b] *University of California, Davis, California 95616*
[c] *University of California Intercampus Institute for Research at Particle Accelerators, Stanford, California 94305*
[d] *University of California, Los Angeles, California 90024*
[e] *University of California, Riverside, California 92521*
[f] *University of California, San Diego, California 92093*
[g] *University of California, Santa Barbara, California 93106*
[h] *Lawrence Berkeley Laboratory, University of California, Berkeley, California 94720*
[i] *Iowa State University, Ames, Iowa 50011*
[j] *University of Massachusetts, Amherst, Massachusetts 01003*
[k] *Max Planck Institute für Kernphysik, Heidelberg, Germany*
[l] *Stanford Linear Accelerator Center, Stanford University Stanford, California 94309*

---

*Work supported in part by Department of Energy contracts DE–FG03–91ER40674, DE–AS03–76ER70285, DE–FG03–91ER40662, DE–AT03–87ER40327, DE–AM03–76SF00010, DE–AC03–76SF00098, DE–FG02–92ER40730, DE–FG02–92ER40715, and DE–AC03–76SF00515), and National Science Foundation grants PHY91–19849 and PHY91–21416.
†Present address: Physics Department, University of Florida, Gainesville, FL 32611.

Abstract

Using data from the TPC/Two-Gamma experiment at PEP, a C=+1 resonance has been observed in the $\pi^+\pi^-\pi^0\gamma$ final state resulting from the fusion of one nearly-real and one quite virtual photon. The actual decay channel is probably $\pi^+\pi^-\pi^0\pi^0$, where one final state photon is not detected, and the mass of the fully-reconstructed state would be approximately 1525 MeV. A four-pion decay mode in turn implies that the resonance has even isospin. The non-observation of this R(1525) when both initial-state photons are nearly-real suggests a spin 1 assignment. Since the large measured value of the product of the branching ratio into $\pi^+\pi^-\pi^0\pi^0$ and the $\gamma\gamma$ coupling makes it unlikely that this state is the mostly– $\bar{s}s$ $f_1(1510)$, its interpretation may lie outside of conventional meson spectroscopy. There is a second, less-significant enhancement observed in the same reaction at a four-pion mass centered around 2020 MeV.

Submitted to Physical Review D

PACS Numbers 14.40.Cs 13.65.+i

I. Introduction

Over the last decade, much progress has been made towards identifying the lowest-lying members of the conventional quark model flavor-SU(3) meson nonets [1]. This is a necessary step before it will be possible to identify positively the spectrum of exotic states such as those composed of four quarks, $\bar{q}qg$ hybrids, or glueballs. Nevertheless, many candidates for such exotic particles have already been found. To cite a relevant example, when LASS confirmed the existence of the mostly– $\bar{s}s$ $f_1(1510)$ in peripheral $K\pi$ interactions [2], the lowest-lying $J^{PC} = 1^{++}$ nonet was completed. However, experiments using central hadronic production [3], radiative J/ψ decays [4], and two-photon interactions [5-9] have indicated that there is at least one spin-one object in the mass region around 1420 MeV. Variously labeled as E(1420), $f_1(1420)$, or X(1420) , such a resonance is surely too low in mass to be an axial vector radial excitation and is thus left with no quark model assignment. Various scenarios have been proposed for the assignment of the X(1420) in the growing experimental compilation of possibly-exotic resonance phenomena [10,11].

There are several reasons why the two-photon reaction, $e^+e^- \rightarrow e^+e^-\gamma\gamma \rightarrow e^+e^-R$, is an excellent tool for conventional meson spectroscopy and for the identification of exotic resonances. First, since the initial state is relatively simple and well-understood, there is less ambiguity in determining the production mechanism than in hadron interactions. Furthermore, the center of mass energy of the reactions is not fixed as in e^+e^- annihilation, thus allowing a range of masses to be probed. Even more important, however, are the constraints on resonance quantum numbers produced in two-photon reactions. The charge conjugation parity of resonances produced by two-photon fusion is unambiguously C = +1. Also, the Yang-Landau theorem [12] states that two massless spin-one objects cannot combine to form a spin-one object. However, when one of the initial spin-one objects is massive, this restriction no longer holds [13]. Thus, when a resonance is not seen in the fusion of two real photons, but is observed when one the photons is far from the mass shell, it indicates that the resonance is probably spin-one [14]. These restrictions are very powerful; they have allowed the recent confirmation of spin-one for the $f_1(1285)$ and X(1420) with only a handful of detected events [5-9].

In this paper we present evidence from the TPC/Two-Gamma experiment at PEP for resonance formation in the fusion of a quasi-real photon and a quite-virtual spacelike photon. Although the enhancements are observed in the $\pi^+\pi^-\pi^0\gamma$ final state, we believe that the true decay mode is $\pi^+\pi^-\pi^0\pi^0$, where one photon from a π^0 decay has gone undetected. In Section II a brief

review of the two-photon fusion process is presented, with emphasis on the production of spin-one objects. Section III describes data collection, event selection and Monte Carlo simulations; it explains why we were led to study the $\pi^+\pi^-\pi^0\pi^0$ final state primarily through the observation of $\pi^+\pi^-\pi^0\gamma$. Evidence for spin-one resonance formation is given in Section IV, along with upper limits on the production of spin-zero resonances and a reexamination of the final state $\pi^+\pi^-\pi^+\pi^-$. Section V discusses the interpretation of these results and Section VI summarizes the paper.

II. Photon-Photon Fusion

Though it has been discussed at length elsewhere, particularly in reference [6], we briefly review the salient points of two-photon resonance formation. Two-photon fusion reactions occur in e^+e^- storage rings when colliding electrons and positrons exchange virtual photons which fuse to form a resonant final state. The invariant mass-squared of photon i (=1,2) is

$$q_i^2 \approx -4\, E_{beam}\, E_i \sin^2\theta_i/2, \qquad (1)$$

where E_i and θ_i are the energy and polar angle of the corresponding scattered leptons in the laboratory frame. Since the flux of virtual photons is approximately proportional to $1/q_i^2$, the scattered leptons will lie predominantly at small angles relative to the beamline and most of the virtual photons will be nearly-real (denoted by γ). When the scattered leptons which would tag the presence and four-momenta of the virtual photons are not detected in the experimental apparatus, the two-photon reaction is called untagged. Correspondingly, the case where one photon is quite virtual (denoted by γ^*) may result in a detectably large scattering angle for the lepton 'tag', leading one to label this two-photon reaction single-tagged. Recall that spin-one mesons can only be produced when at least one of the photons is virtual; thus one would expect the signature of such particles in a two-photon experiment to be production in single-tagged, but not in untagged, reactions.

The general cross section for formation of a resonance — with mass M_R, total width Γ_0, and spin J — by two-photon fusion is [15]

$$\sigma_{AB} = \frac{32\pi\,(2J+1)}{N_A\,N_B}\left(\frac{W^2_{\gamma^*\gamma^*}}{2\sqrt{X}}\right)\left[\frac{\Gamma_0}{\left(W^2_{\gamma^*\gamma^*} - M_R^2\right)^2 + M_R^2\Gamma_0^2}\right]\Gamma^{AB}_{\gamma^*\gamma^*}\,(q_1^2,\, q_2^2,\, W^2_{\gamma^*\gamma^*}) \qquad (2)$$

where $X \equiv (q_1 \cdot q_2)^2 - q_1^2 q_2^2$, and $W^2_{\gamma^*\gamma^*} \equiv (q_1 + q_2)^2$ is the square of total invariant mass of the $\gamma^*\gamma^*$ system. The symbols A and B stand for polarization states of the two virtual photons, either

longitudinal (L) or transverse (T), with $N_L=1$ and $N_T=2$. When a resonance is produced in untagged two-photon fusion, both photons are nearly real and thus transversely polarized, so there is only one two-photon cross section, σ_{TT}. Measurement of this cross section determines the radiative width, $\Gamma_{\gamma\gamma}(R)$, defined by

$$\Gamma_{\gamma\gamma}(R) = \Gamma^{TT}_{\gamma^*\gamma^*}(0,0,M_R^2). \tag{3}$$

However, for single-tagged two-photon fusion, where $Q^2 \equiv \max(|q_1^2|,|q_2^2|)$ is large, there can be two distinct two-photon cross sections, σ_{TT} and σ_{LT}, with different Q^2 dependences. In the specific case of the formation of a pseudoscalar particle P (with mass M_P), for which $\sigma_{LT}=0$, one defines a single form factor, $F(Q^2)$, by

$$\Gamma^{TT}_{\gamma^*\gamma}(Q^2) = \frac{4X}{M_P^4} F^2(Q^2)\Gamma_{\gamma\gamma}(P) \ . \tag{4}$$

The form factor is often parametrized in the vector dominance manner:

$$F(Q^2) = \left[1+\frac{Q^2}{m_V^2}\right]^{-1} , \tag{5}$$

where m_V is the mass of one of the vector mesons (i.e. ρ, ϕ,...). However, for general resonance production, it is not theoretically well understood how the two cross sections are related. To parametrize this for a spin-one resonance, R, one can define the effective two-photon width measured in single-tagged experiments:

$$\Gamma_{\gamma^*\gamma}(Q^2) = \left[1+\varepsilon^{-1}R\,(Q^2)\right]\Gamma^{LT}_{\gamma^*\gamma}(Q^2), \tag{6}$$

where ε^{-1} (≈ 1 for our experiment) is the ratio of the TT to LT two-photon luminosity functions [15], and the ratio of the distinct cross-sections, $R(Q^2) = \sigma_{TT}/\sigma_{LT}$, is model dependent. Since, for a spin-one resonance, Yang's theorem implies

$$\text{as } Q^2 \to 0, \quad \Gamma^{TT}_{\gamma^*\gamma}(Q^2) \to 0 \ , \tag{7}$$

we define — in analogy with (3) — the two-photon coupling parameter, $\tilde{\Gamma}_{\gamma\gamma}(R)$, such that

$$\text{as } Q^2 \to 0, \quad \frac{M_R^2}{Q^2}\Gamma^{LT}_{\gamma^*\gamma}(Q^2) \to \tilde{\Gamma}_{\gamma\gamma}(R), \tag{8}$$

and the effective form factor, $\tilde{F}\ (Q^2)$, by

$$\Gamma_{\gamma^*\gamma}(Q^2) = \frac{4X}{M_R^4}\tilde{F}^2(Q^2)\tilde{\Gamma}_{\gamma\gamma}(R)\ . \qquad (9)$$

For the two-photon formation of a conventional axial vector ($J^{PC} = 1^{++}$) meson with mass M_A, we use a theoretical model of Cahn [16,17] which predicts that $R(Q^2) = Q^2 / 2\ M^2_A$ (for small Q^2), leading to

$$\tilde{F}^2(Q^2) = \left[1 + \frac{Q^2}{2m_A^2}\right]\frac{Q^2}{m_A^2}F^2(Q^2)\ . \qquad (10)$$

Note that as Q^2 --> 0, $\Gamma_{\gamma^*\gamma}(Q^2)$ approaches the two-photon width for even-spin resonances but goes to zero for spin-one resonances. This provides a clean method for distinguishing the spin of the produced particle in single-tagged reactions, even with low statistics, so long as the experiment can tag small Q^2 events.

III. Data, Analysis, and Simulation

Since the analysis described here follows closely that of reference [6], we briefly review the common elements and discuss in detail only those parts of the analysis unique to the $\pi^+\pi^-\pi^0\pi^0$ and $\pi^+\pi^-\pi^0\gamma$ final states [18].

The data were collected by the TPC/Two-Gamma detector [19] at the electron-positron storage ring PEP at SLAC, with a center-of-mass energy of 29 GeV/c^2. The integrated luminosities were 140 pb^{-1} for untagged data and 114 pb^{-1} for single-tagged data. The Time Projection Chamber (TPC) was used in coordination with a solenoidal magnetic field to detect charged particles and simultaneously measure their momenta, **p**, and rate of energy loss, dE/dx. There was additional charged track detection provided by fifteen planes of drift chambers in the forward regions between 25 and 180 mrad from the beam direction. Tags were detected and their energies measured with either a sodium-iodide array (NaI) covering 25 to 90 mrad or a lead/scintillator calorimeter (SHW) between 100 and 180 mrad from the beam direction. Photons were detected by either a hexagonal-barrel calorimeter (HEX) operating in the Geiger mode and covering angles larger than 700 mrad from the beam, a proportional-mode pole-tip calorimeter (PTC) covering from 300 to 600 mrad, or the NaI or SHW calorimeters from 25 to 180 mrad. Photons which converted in the material between the interaction point (IP) and the TPC were reconstructed if the

e^+e^- pair was detected within the TPC. In the untagged data the trigger required at least two charged tracks in separated TPC sectors, or one charged track in the TPC combined with a large energy deposition in either the HEX or PTC. In the single-tagged data, the trigger fired on events which had either a tag plus at least one track in the TPC, or a tag plus a large energy deposition in either the HEX or PTC.

In selecting $\pi^+\pi^-\gamma\gamma\gamma\gamma$ and $\pi^+\pi^-\gamma\gamma\gamma$ events, there had to be two oppositely-charged tracks with p >100 MeV/c observed in the TPC, both originating from the interaction point and each having p and dE/dx values consistent with a $\pi^\pm$ hypothesis. We also required three (or four) showers with energies greater than 70 MeV (50 MeV) in the HEX, 150 MeV in the PTC, 250 MeV in the NaI, 500 MeV in the SHW, or 50 MeV for photons observed in the TPC as conversion pairs. The showers had to be detected in the well-understood regions of the calorimeters, and separated from the projections of tracks by at least 400 mrad in the HEX and 120 mrad in the PTC. In the single-tagged case, we required the observation of a large energy deposition in either the NaI ($E_{tag} \geq 4$ GeV/c^2) or SHW ($E_{tag} \geq 8$ GeV/c^2) forward calorimeters, with evidence of an associated charged track in the forward drift chambers.

The $\gamma\gamma$ invariant mass spectrum from the single-tagged $\pi^+\pi^-\gamma\gamma\gamma$ data, shown in Fig. 1a, demonstrates a broad peak at the π^0 mass, with substantial combinatorial background, since there is as yet no attempt to determine which of the photons is paired with the presumed missing photon. To accomplish this, we performed three separate one constraint (1C) fits with hypotheses $m_{12} = m_{\pi^0}$, $m_{13} = m_{\pi^0}$, and $m_{23} = m_{\pi^0}$, respectively. If none of these assignments passed the fit with better than 2% confidence, then the event was rejected. If just one assignment passed the fit, then that pair of photons was taken to be the π^0. If more than one assignment passed the fit, then the π^0 was taken to be that pair with the lowest value of $|\cos\alpha_{ij} - \cos\beta_{ij}|$, where α_{ij} is the opening angle between γ_i and γ_j, while β_{ij} is the prediction of this opening angle given the γ energies:

$$\cos\beta_{ij} = 1 - \frac{m_\pi^2}{2E_iE_j} \tag{11}$$

Fig. 1b shows the $\gamma\gamma$ invariant mass spectrum for the single-tagged $\pi^+\pi^-\gamma\gamma\gamma$ events surviving both this algorithm and a net transverse momentum cut of 250 MeV/c. The latter cut facilitates comparison with a Monte Carlo simulation of the same spectrum generated from the two-photon production of $\pi^+\pi^-\pi^0\pi^0$, using a W-independent cross section and isotropic decay [20]. The events from this and from all other Monte Carlo simulations described herein were passed through a complete detector simulation, which included the effects of nuclear and electromagnetic interactions with detector materials, as well as inefficiencies due to detector response, triggering, event selection and fitting procedures. The shape and width of the π^0 peak are primarily due to

detector energy resolution. From a study of these Monte Carlo events, the above algorithm was determined to be about 85% accurate in making the correct assignments. These simulations also showed that about 60% of the undetected photons had energies below the detector thresholds, 18% were not significantly separated from other photons and so were merged with them, 15% escaped detection by going through a crack in the detector, and 7% were lost by being associated with tracks.

Analysis of the fully-reconstructed final state $\pi^+\pi^-\gamma\gamma\gamma\gamma$ proceeded similarly, although the number of events was smaller and the combinatorial background was worse. To reduce the background in this case, we performed three two-constraint (2C) fits with hypotheses of the form $m_{ij} = m_{\pi 0}$ and $m_{kl} = m_{\pi 0}$ and chose that assignment with the smallest value of $(\cos \alpha_{ij} - \cos \beta_{ij})^2 + (\cos \alpha_{kl} - \cos \beta_{kl})^2$. According to Monte Carlo studies, this method was more than 95% accurate in selecting the correct photon pairs for each π^0.

Figure 2 shows the net transverse momentum squared, p_t^2, distribution (tag included) for the single-tagged $\pi^+\pi^-\pi^0\gamma$ and $\pi^+\pi^-\pi^0\pi^0$ data samples, together with the prediction of the Monte Carlo simulation described above. For the $\pi^+\pi^-\pi^0\gamma$ events, a rather stringent requirement that the net transverse momentum be less than 250 MeV/c was then imposed to reject non-exclusive background, even though the Monte Carlo simulation shows that this resulted in about a 20% loss of signal due to the missing photon. The fully-reconstructed $\pi^+\pi^-\pi^0\pi^0$ spectrum shows a sharper peak at smaller p_t^2, as would be expected for exclusive two-photon events. Here we made a looser cut of $p_t < 300$ MeV/c, but then subjected the events to a four-constraint (4C) fit, where we demanded that the net transverse momentum be consistent with zero within the resolution.

The detection efficiencies for events analyzed in the above manner were determined through Monte Carlo studies. A variety of decay chains from spin-zero and spin-one resonances leading to the $\pi^+\pi^-\pi^0\pi^0$ final state were modeled, including the four-body phase space decay of a spin-zero resonance, $\rho^+\rho^-$ or $\rho^+\pi^-\pi^0$ production with $\rho^+ \rightarrow \pi^+\pi^0$, and $a_1(1260)\pi$ in isoscalar and isotensor states with a_1 decaying to three pions. This was done [18] by re-weighting the $\pi^+\pi^-\pi^0\pi^0$ phase space cross sections with the appropriate matrix elements, using the square root of the running width and a suitable centrifugal factor as proposed by Jackson [21]. Helicity and angular momentum were conserved at every vertex with the proper combinations of spherical harmonics, and intermediate states were propagated with the appropriate Breit-Wigner amplitudes. Figure 3 depicts the detection efficiencies as a function of $W_{\gamma^*\gamma^*}$ for single-tagged $\pi^+\pi^-\pi^0\pi^0$ and $\pi^+\pi^-\pi^0\gamma$ final states from one such model, that of spin-zero production with phase space decay to four pions. Other spin-zero models led to results which were not systematically different, while detection efficiencies for spin-one models were consistently larger by factors ranging from 1.4 at 1.3 GeV to 1.15 at 2.0 GeV, because the spin-one events preferentially populated higher Q^2

regions where the detector coverage and triggering were better. In all cases, the detection efficiency was several times larger for the case where one photon is undetected than for the exclusive final state, and thus most of the results presented in this paper come from the study of $\pi^+\pi^-\pi^0\gamma$ rather than $\pi^+\pi^-\pi^0\pi^0$.

IV. Results

Figure 4 is a plot of the invariant mass of the single-tagged $\pi^+\pi^-\pi^0\gamma$ system, showing clear evidence for a peak in the neighborhood of 1400 MeV, and a broad enhancement between 1700 and 2150 MeV. In contrast, the untagged invariant mass spectrum shown in Fig. 5 contains no sign of resonant activity. As discussed in Section II, if we can establish that a peak in the single-tagged spectrum is indeed a resonance, its absence in the untagged spectrum would imply that the spin of the resonance is odd (most likely spin-one for a low-mass resonance). A fit of the single-tagged spectrum in Fig. 4 with a single Breit-Wigner shape and a third-order polynomial background gives a mass of 1432 ± 21 MeV, although the background is unable to accommodate the shape on the high side of the peak. A better fit can be obtained by using a polynomial background and two Breit-Wigners, with masses of 1410 ± 20 and 1920 ± 50 MeV. However, it seems likely that Fig. 4 does not represent exclusive $\pi^+\pi^-\pi^0\gamma$ production but rather $\pi^+\pi^-\pi^0\pi^0$, where one of the photons from the decay of a π^0 was not detected. As noted previously, Monte Carlo simulations suggest that this is a probable result of our relatively high calorimeter energy thresholds, incomplete calorimeter coverage, and merging of photon showers. Furthermore, although we cannot rule it out, it seems unlikely that a hadron in this high-mass region would itself have a dominant radiative decay mode. One might speculate that there are intermediate states in the decay chain with significant radiative decay modes such as η, η', or ω. However, as can be seen in Figs. 6 and 7 for the regions of the two enhancements, there is no evidence for such decay products in any of the invariant mass combinations. Indeed, the only indications of intermediate structure are possible ρ peaks in Figs. 6a,c and a likely charged ρ in Fig. 7c. Henceforth, we assume that the true final state is actually $\pi^+\pi^-\pi^0\pi^0$ [22].

With one photon undetected, the shapes of the peaks in the $\pi^+\pi^-\pi^0\gamma$ invariant mass spectrum are distorted and our fits underestimate the actual $\pi^+\pi^-\pi^0\pi^0$ masses. Figure 8 presents the peak $\pi^+\pi^-\pi^0\gamma$ invariant mass which would be observed as a function of the true $\pi^+\pi^-\pi^0\pi^0$ mass, where the points come from a variety of the Monte Carlo models described earlier. The dashed lines are at the observed masses of the enhancements of Fig. 4, and the dotted lines give an indication of the uncertainty due to model dependence. Thus, the peak seen in the $\pi^+\pi^-\pi^0\gamma$ spectrum at about 1410 MeV would have an actual $\pi^+\pi^-\pi^0\pi^0$ mass of about 1525 MeV, and the broad enhancement

seen at about 1920 MeV with one photon missing would be centered at about 2020 MeV in the fully-reconstructed state.

In order to perform proper fits to the $\pi^+\pi^-\pi^0\gamma$ spectrum, we used Monte Carlo studies to deduce a resonance shape which results from a Breit-Wigner $\pi^+\pi^-\pi^0\pi^0$ shape, but with only $\pi^+\pi^-\pi^0\gamma$ reconstructed. The distorted shape of such a resonance was found to be largely independent of the spin or decay mode used in the generation of Monte Carlo events. The detector resolution for the fully-reconstructed final state is about 120 MeV (FWHM) at a mass of 1525 MeV and about 170 MeV at a mass of 2020 MeV, whereas a Gaussian fit to the distorted Monte Carlo shape with one undetected photon gives a width of about 280 MeV independent of mass. Given this poor mass resolution, it is very difficult to ascertain the intrinsic width of any resonances in Fig. 4. For fitting purposes, we chose to use two Breit-Wigner resonances with fixed masses and intrinsic widths as Monte Carlo inputs: a Γ_0=1 MeV peak at 1525 MeV and a Γ_0=200 MeV peak at 2020 MeV. The fits also included a third order polynomial to represent the background shape. We obtained 97 ± 15 events for the peak at a $\pi^+\pi^-\pi^0\pi^0$ mass of 1525 MeV, and 82 ± 20 events for the enhancement around a $\pi^+\pi^-\pi^0\pi^0$ mass of 2020 MeV. To determine the statistical significance of a given peak, we performed a separate fit which included all contributions except the Monte Carlo shape for that peak. Such fits gave a statistical significance for the lower peak of 7.5 standard deviations and a statistical significance for the upper peak of 3.3 standard deviations.

There are two known $\bar{q}q$ states, the $f_1(1285)$ and the $f_2(1270)$, which have small, but significant, branching fractions to $\pi^+\pi^-\pi^0\pi^0$ and thus should appear in the single-tagged $\pi^+\pi^-\pi^0\gamma$ mass spectrum. A Monte Carlo calculation of the expected contribution from the $f_2(1270)$ yields 14 ± 6 events, given the known branching fraction to $\pi^+\pi^-\pi^0\pi^0$ [1]. To calculate the expected contribution from the $f_1(1285)$, we need both the known branching fraction to four pions (0.38 ± 0.04) [1], and the unknown fraction of this resulting in $\pi^+\pi^-\pi^0\pi^0$, which can vary from 0.44 for no intermediate ρ content to 0.67 for a $\rho\rho$ intermediate state. Thus, the net branching fraction for $f_1(1285) \rightarrow \pi^+\pi^-\pi^0\pi^0$ lies between 0.17 and 0.25 which, from our previous measurement [6] of its $\gamma\gamma$ formation cross section and from the acceptance for $f_1(1285) \rightarrow \pi^+\pi^-\pi^0\gamma$, leads to a prediction of 23 ± 11 $f_1(1285)$'s in the $\pi^+\pi^-\pi^0\gamma$ spectrum. When the shapes from a Monte Carlo simulation of the $f_1(1285)$ and the $f_2(1270)$ are included in the fitting procedure, together with those of the two peaks described above and the third order polynomial background, we obtain 14 ± 28 $f_1(1285)$ events, 1 ± 37 $f_2(1270)$ events, 95 ± 15 events for the peak at a corrected mass of 1525 MeV, and 90 ± 21 events for the enhancement around a corrected mass of 2020 MeV. This fit, shown in Fig. 9 as the histogram along with the data from Fig. 4 (now plotted as points with error bars), yields numbers for the $f_1(1285)$ and $f_2(1270)$ which are consistent with expectations,

albeit very uncertain due to the poor mass resolution. We use these fit numbers in all further analysis.

We have tried fitting using many other, more complicated, background shapes, none of which led to a significantly better fit than the polynomial background. One can attempt to derive a less-arbitrary background shape by fitting the untagged $\pi^+\pi^-\pi^0\gamma$ spectrum (points with error bars) with a 4th order polynomial (solid curve) as shown in Fig. 10. In order to obtain a background shape appropriate for single-tagged data, one must scale that curve by calculated, mass-dependent ratios of single-tagged to untagged $\gamma\gamma$ luminosity functions and acceptances, by an overall e^+e^- luminosity ratio, and by an assumed ratio of $\gamma\gamma$ cross sections. The latter depends upon a choice of form factors and a model for the relative contributions of different spins. If one assumes that the background is dominated by spin-0, and uses the same ρ-pole form factor at all masses, the result is the dashed curve on Fig. 9. Both enhancements clearly stand out above this background, with statistical significances of 7.1 standard deviations for the lower peak and 6.2 standard deviations for the upper peak. Given that this and every reasonable background we have tried leads to at least 5 standard deviation significance for the lower mass peak, we conclude that we have observed one new resonance, the R(1525). We use the range of values obtained from fits performed with different backgrounds and resonance widths to derive a systematic error of 30% on the number of R(1525) events. On the other hand, the sensitivity of the higher mass enhancement to different background shapes, and the generally lower statistical significance (as low as 3 standard deviations), allows us only to say that there is a possibility of one or more resonances which we generically label as R(2020).

Since we have observed resonance formation in the $\pi^+\pi^-\pi^0\gamma$ final state, which we believe originates from $\pi^+\pi^-\pi^0\pi^0$ with one photon undetected, it is important to examine the small sample of fully-reconstructed $\pi^+\pi^-\pi^0\pi^0$ events shown in Fig. 11 and Fig. 12, for single-tagged and untagged production, respectively. The solid curve in Fig. 11 was obtained by performing a quadratic fit to the data and the solid curve in Fig. 12 is a fourth-order polynomial fit. The dashed curve in Fig. 11 is the result of scaling the untagged background curve from Fig. 12, in the same manner described previously for Figs. 9 and 10. The histogram in Fig. 11 is the result of adding two Monte Carlo peak shapes to the solid curve, where the peaks were generated with the same masses and intrinsic widths as noted earlier and are normalized by scaling the numbers of events in the fit peaks of the $\pi^+\pi^-\pi^0\gamma$ sample by the spin-one acceptance ratio of single-tagged $\pi^+\pi^-\pi^0\pi^0$ to $\pi^+\pi^-\pi^0\gamma$. The single-tagged $\pi^+\pi^-\pi^0\pi^0$ spectrum is statisically consistent with the signals seen in $\pi^+\pi^-\pi^0\gamma$. No other two-photon experiment has published results from single-tagged $\pi^+\pi^-\pi^0\pi^0$ production.

The observation of a peak in a single-tagged mass spectrum, and its absence in the corresponding untagged mass spectrum, is the hallmark of odd-spin resonance formation in two-photon reactions, as discussed earlier. The most likely assignment for a low-mass resonance observed in this manner, such as the R(1525), would be spin-one [14]. If this spin-one interpretation were incorrect, and the observed enhancements in the single-tagged $\pi^+\pi^-\pi^0\gamma$ spectrum were spin-zero, the histograms in Fig. 10 and Fig. 12 indicate what should be observed in the untagged spectra (assuming a ρ-pole form factor). Clearly no such large signals are seen in either untagged data set. Combined fits to the data in Figs. 9 and 10, using spin-zero Monte Carlo histograms together with various polynomial background shapes, yielded a maximum probability of less than 0.1%, whereas the fit to the mass-dependence of Fig. 9 alone had a confidence level of 98%. Thus the R(1525) is most likely spin-one.

In order to derive the Q^2 dependence of R(1525) production, we separated the single-tagged $\pi^+\pi^-\pi^0\gamma$ data into five bins in Q^2 and repeated the mass fitting procedure described above for Fig. 9. The numbers of events assigned to the R(1525) signal were then corrected for acceptance to yield the evolution of the e^+e^- --> e^+e^-R(1525) cross section with Q^2 as shown in Fig. 13a. The resulting two-photon coupling parameter times effective form factor squared, assuming $J_R = 1$ and the Cahn model (see eqs. 9 and 10), is plotted in Fig. 13b. Using the integrated number of events [23] and two different form factor assumptions, we derive the branching ratio times two-photon coupling parameter for the spin-1 hypothesis:

$$J=1,\ \rho\ pole \Rightarrow\ BR(R(1525)\rightarrow\pi^+\pi^-\pi^0\pi^0)\times\tilde{\Gamma}_{\gamma\gamma}(R(1525)) = 4.1\pm0.8\pm1.4\ keV \qquad (12)$$

$$J=1,\ \phi\ pole \Rightarrow\ BR(R(1525)\rightarrow\pi^+\pi^-\pi^0\pi^0)\times\tilde{\Gamma}_{\gamma\gamma}(R(1525)) = 2.6\pm0.5\pm0.9\ keV \qquad (13)$$

where the TPC/Two-Gamma convention [17] is used. In each case, the first error is statistical and the second systematic. The contributions to the 35% systematic error include 16% from the simulation of the acceptance and event selection, 30% from uncertainties in background shapes and resonance widths, and 7% from the determination of the integrated luminosity. Our previous results for other spin-one states using this model were: $\tilde{\Gamma}_{\gamma\gamma}(f_1(1285)) = 2.4\pm0.5\pm0.5\ keV$ (with a ρ-pole form factor), and $BR(X(1420)\rightarrow KK\pi)\times\tilde{\Gamma}_{\gamma\gamma}(R(1420)) = 1.3\pm0.5\pm0.3\ keV$ (with a ρ-pole form factor) or $BR(X(1420)\rightarrow KK\pi)\times\tilde{\Gamma}_{\gamma\gamma}(R(1420)) = 0.63\pm0.24\pm0.15\ keV$ (with a φ-pole form factor) [6]. Thus, the R(1525) appears to have a large coupling to $\gamma\gamma^*$. The solid (dashed) curve in Fig. 13b is the prediction of the Cahn model with a ρ-pole (φ-pole) form factor, given the measured couplings. The size of the statistical and systematic errors make it impossible to differentiate between these form factor choices with our data. Note that while the cross section

results in Fig. 13a are relatively independent of the Monte Carlo model, the values for the two-photon coupling parameter in Fig. 13b and in (12) and (13) are very sensitive to the choice of model. The Cahn model is only really applicable at low Q^2 and may not be an appropriate description over our whole Q^2 range. The Cahn model is also explicitly for axial vector $\bar{q}q$ mesons and thus may not even apply to the R(1525).

Finally, given our claim for single-tagged resonance formation and decay into $\pi^+\pi^-\pi^0\pi^0$, it is natural to reinvestigate the single-tagged $\pi^+\pi^-\pi^+\pi^-$ channel [6] . This invariant mass spectrum, shown in Fig. 14, gives no clear evidence for resonances, although there is structure in both mass regions (around 1500 and 2000 MeV). However, this is a very difficult channel for resonance searches because it is dominated by the large cross section for $\rho^0\rho^0$ production [24-28], for which no completely convincing models have yet been developed. We therefore used the rather arbitrary smooth curve shown in Fig. 14 as a conservatively low background shape for calculating upper limits:

$$J=1,\ \rho\ pole \Rightarrow\ BR(R(1525)\rightarrow\pi^+\pi^-\pi^+\pi^-)\times\tilde{\Gamma}_{\gamma\gamma}(R(1525))\leq 1.9\ keV,\ (95\%\ \text{C.L.}) \quad (14)$$

$$J=1,\ \rho\ pole \Rightarrow\ BR(R(2020)\rightarrow\pi^+\pi^-\pi^+\pi^-)\times\tilde{\Gamma}_{\gamma\gamma}(R(2020))\leq 2.1\ keV,\ (95\%\ \text{C.L.}) \quad (15)$$

Only the PLUTO experiment has previously published [26] a single-tagged $\pi^+\pi^-\pi^+\pi^-$ mass spectrum from two-photon interactions and, with about 1/3 of our statistics, it shows no significant resonance activity.

V. Interpretation

If the R(1525) is indeed a new resonance, it is interesting to speculate on its nature. There are four known [1] C=+1 states in this mass region: $f_1(1510)$, $f_0(1525)$, $f_2(1520)$ and $f_2'(1525)$ [29]. The latter three states are even-spin resonances, which should appear in untagged two-photon reactions if they appear in single-tagged production, and none of them has a significant four-pion decay mode. The $f_1(1510)$ appears to be a mostly-$\bar{s}s$ resonance, since it has been seen only to decay to K*K [2]. If so, its formation in two-photon reactions should be suppressed [31], because the cross section is proportional to the 4th power of quark charge, whereas we have demonstrated that the R(1525) has a particularly large two-photon coupling. Since it seems reasonable to assume that the $f_1(1510)$ completes the lowest lying $J^{PC} = 1^{++}$ nonet [1], and the R(1525) is likely too low

in mass to be an axial vector radial excitation [30], then the R(1525) is a candidate for a $\bar{q}qg$ or $\bar{q}^2q^2$ state.

There are already several possible exotic states in the mass region around 1500 MeV. Mark III and DM2 have seen evidence [32], in radiative J/ψ decays to $\pi^+\pi^-\pi^+\pi^-$ and $\pi^+\pi^-\pi^0\pi^0$ final states, for a resonance with a mass between 1450 and 1550 MeV. However, they both favor a ρρ intermediate state and a pseudoscalar assignment, while our R(1525) has only weak evidence for ρ content (Fig. 6a,c) and appears to be spin-one. The hadronic 'central production' experiment WA76, which often sees the same resonances as in two-photon interactions, has detected [33] a state with a mass of 1449 MeV and a width of 78 MeV which decays dominantly to $\rho^0\pi^+\pi^-$ and likely has spin either one or two. However, the mass difference between the WA76 peak and our R(1525) makes it unlikely that they are the same state. Finally, GAMS [34] observes a G(1590) resonance in the $4\pi^0$ final state, but it is either a tensor or a scalar, not an axial vector. Thus, none of these resonances matches our R(1525) observation very well.

Further evidence on the nature of this resonance might be obtained if its isospin assignment could be determined. The formation of R(1525) in γγ reactions implies C=+1 and the inferred four-pion decay mode then requires isospin, I_R, even by G-parity conservation. Making the most reasonable assumption of $I_R = 0$ would give bounds on the ratio of cross sections:

$$\frac{1}{2} \leq \frac{\sigma(\pi^+\pi^-\pi^0\pi^0)}{\sigma(\pi^+\pi^-\pi^+\pi^-)} \leq 2. \qquad (16)$$

Comparing the upper limit (14) with (12) shows that our measurements are consistent with this range. If it could be shown definitively that the R(1525) were observed in the $\pi^+\pi^-\pi^0\pi^0$ channel but not in the $\pi^+\pi^-\pi^+\pi^-$ channel, then one would have to consider another isospin assignment. For example, there are isotensors (e.g. $I_{total} = 2$, $I_{12} = 1$, $I_{34} = 2$) which decay 100% to $\pi^+\pi^-\pi^0\pi^0$ and others which have some small admixture of $\pi^+\pi^-\pi^+\pi^-$. Such an isospin assignment cannot be attained from a conventional bound $\bar{q}q$ state, but is possible for a $\bar{q}^2q^2$ state.

If the broad enhancement which we tentatively label the R(2020) is found to be a resonance, there are many possibilities for its interpretation, including a radially- or orbitally- excited $\bar{q}q$ meson, or an exotic state. Radiative J/ψ data [32] for $\pi^+\pi^-\pi^+\pi^-$ and $\pi^+\pi^-\pi^0\pi^0$ final states show evidence for resonances at around 1800 and 2100 MeV, although the data suggest a pseudoscalar interpretation. The WA76 collaboration [33], using central hadronic interactions, has observed a broad structure in $\pi^+\pi^-\pi^+\pi^-$ at a mass of 1900 MeV/c^2 which might explain the lower part of our enhancement, although they indicate that the intermediate states $a_2(1320)\pi$ and $f_2(1270)\pi\pi$ are dominant and we do not see evidence for those. GAMS [34] observes an X(1850) tensor resonance in the $4\pi^0$ final state, although Crystal Ball has seen no evidence for this, or any other

high-mass resonance, in two-photon reactions to the same final state [35]. There are several other established resonances [1] with masses in the 2000-2200 MeV range which might contribute to the upper part of the enhancement, although all of them have spin-parity assignments which should allow their detection in untagged reactions as well.

VI. Conclusions

Using 140 pb^{-1} of untagged data and 114 pb^{-1} of single-tagged data accumulated by the TPC/Two-Gamma experiment at the SLAC storage ring PEP, we have studied the reaction $\gamma\gamma^{(*)} \rightarrow \pi^+\pi^-\pi^0\pi^0 \rightarrow \pi^+\pi^-\gamma\gamma(\gamma)$, where one of the final-state photons could be undetected. A resonance was observed in the single-tagged $\pi^+\pi^-\pi^0\gamma$ data, with a statistical significance of at least five standard deviations. We believe that the actual decay channel is $\pi^+\pi^-\pi^0\pi^0$ and the peak mass for fully-reconstructed events would be approximately 1525 MeV/c^2. The $\pi^+\pi^-\pi^0\pi^0$ spectrum is consistent with the presence of this R(1525), although there are too few such fully-reconstructed events to prove its presence. Formation of such a resonance in two-photon reactions requires C=+1 and the strong decay to $\pi^+\pi^-\pi^0\pi^0$ implies even isospin. No signal was observed in the untagged data samples, indicating the probable spin-one nature of the R(1525). No definitive signals were seen in the single-tagged $\pi^+\pi^-\pi^+\pi^-$ data sample, although the large $\rho^0\rho^0$ cross section obscures this mass region in that channel. The R(1525) is not consistent with any known resonance; its mass and quantum numbers make it a candidate for a non– $\bar{q}q$ meson. An additional enhancement, centered around a $\pi^+\pi^-\pi^0\pi^0$ mass of 2020 MeV/c^2, was observed with marginal statistical significance in the single-tagged $\pi^+\pi^-\pi^0\gamma$ spectrum.

Acknowledgments

We gratefully acknowledge the efforts of the PEP staff for their dedication and productive running of the machine, and the engineers and technicians of the collaborating institutions for their efforts in the construction and maintenance of the detector. This work was supported in part by the United States Department of Energy (under contracts DE-FG03-91ER40674, DE-AS03-76ER70285, DE-FG03-91ER40662, DE-AT03-87ER40327, DE-AM03-76SF00010, DE-AC03-76SF00098, DE-FG02-92ER40730, DE-FG02-92ER40715, and DE-AC03-76SF00515), and the National Science Foundation (under grants PHY91-19849 and PHY91-21416).

References

1. K. Hikasa *et al.*, Particle Data Group, *Phys. Rev.* **D45**, 1 (1992). For a recent review of resonances produced in two-photon interactions, see H. Kolanoski, *Proceedings of the IX International Workshop on Photon-Photon Collisions,* San Diego, CA, March 1992, ed. D. Caldwell and H. Paar (World Scientific, Teaneck, N.J., 1993), pg.3.

2. D. Aston *et al.*, LASS collaboration, *Phys. Lett.* **B201**, 573 (1988).

3. T.A. Armstrong *et al.*, WA76 collaboration, *Phys. Lett.* **B221**, 216 (1989) and *Z. Phys.* **C34**, 23 (1987).

4. Z. Bai *et al.*, Mark-III collaboration, *Phys. Rev. Lett.* **65**, 2507 (1990) and J.E. Augustin, *et al.*, DM2 collaboration, *Phys. Rev.* **D42**, 10 (1990).

5. H. Aihara, *et al.*, TPC/Two-Gamma collaboration, *Phys. Rev. Lett.* **57**, 2500 (1986).

6. H. Aihara, *et al.*, TPC/Two-Gamma collaboration, *Phys. Rev.* **D38**, 1 (1988).

7. G. Gidal *et al.*, Mark-II collaboration, *Phys. Rev. Lett.* **59**, 2016 (1987).

8. P. Hill *et al.*, Jade collaboration, *Z. Phys.* **C42**, 355 (1989).

9. H.J. Behrend *et al.*, Cello collaboration, *Z. Phys.* **C42**, 367 (1989).

10. D. O. Caldwell, *Mod. Phys. Lett.* **A2**, 771 (1987).

11. M. Chanowitz, *Phys. Lett.* **B187**, 409 (1987).

12. L. F. Landau, *Dok. Akad. Nauk USSR* **60**, 207 (1948); C. N. Yang, *Phys. Rev.* **77**, 242 (1950).

13. F. M. Renard, *Il Nuovo Cimento* **80A**, 1 (1984).

14. For resonances produced in the fusion of two real photons, the full set of selection rules derived from gauge invariance, parity conservation, Bose symmetry and Lorentz invariance is $\sigma_{\gamma\gamma\to R}$ ($J^P = 1^+, 1^-, 3^-, 5^-, 7^-, ...$) = 0. See, for example, M. Poppe, *Int. J. Mod. Phys.* **1**, 545 (1986). Although a resonance produced only when one of the photons is quite virtual could have any of the odd spins, it is expected that the spin-1 meson nonets are less massive than those with higher spins.

15. V. M. Budnev, I. F. Ginzburg, G. V. Meledin, and V. G. Serbo, *Phys. Rep.* **15C**, 181 (1975).

16. R. N. Cahn, *Phys. Rev.* **D35**, 3342 (1987) and **D37**, 833 (1988); note that this model is explicitly for $\bar{q}q$ mesons ($J^{PC} = 1^{++}$) and would likely not apply to the case of hybrid $\bar{q}qg$ production ($J^{PC} = 1^{-+}$).

17. We use the TPC/Two-Gamma convention (also adopted by the PDG in reference 1) for the definition of two-photon coupling parameters, which results in values which are half those of reference 16; see reference 6 for further details.

18. Ransom W. Stephens, Ph.D. thesis, University of California, Santa Barbara, 1990 (unpublished).

19. H. Aihara *et al.*, Lawrence Berkeley Laboratory Report No. LBL-23737, 1988 (unpublished).

20. Note that the small width of the π^0 peak in this Monte Carlo model, as compared with that in the data, is primarily due to the use of the W-independent cross section over a large range ($0.8 < W < 2.8$ GeV). A Monte Carlo simulation for a resonance at a mass of 1525 MeV, with a decay to $\pi^+\pi^-\pi^0\pi^0$, gives better agreement with the π^0 peak seen in the data.

21. J. D. Jackson, *Il Nuovo Cimento* **34**, 1644 (1964).

22. We cannot exclude some contribution from the final states $\pi^+\pi^-\pi^0\pi^0\pi^0$ and $\pi^+\pi^-\pi^0\eta$, although there is no evidence for η production in Fig. 1 and the p_t cut should discriminate against these final states much more than against $\pi^+\pi^-\pi^0\pi^0$.

23. One can also derive values for the two-photon coupling parameter from fits to Fig. 13b; these agree with the quoted values within the uncertainties.

24. H. Albrecht *et al.*, Argus collaboration, *Z. Phys.* **C50**, 1 (1991).

25. H. Aihara *et al.*, TPC/Two-Gamma collaboration, *Phys. Rev.* **D37**, 28 (1988).

26. Ch. Berger *et al.*, Pluto collaboration, *Z. Phys.* **C38**, 521 (1988)

27. H.J. Behrend *et al.*, Cello collaboration, *Z. Phys.* **C21**, 205 (1984).

28. M. Althoff *et al.*, Tasso collaboration, *Z. Phys.* **C16**, 13 (1982); and R. Brandelik *et al.*, Tasso collaboration, *Phys. Lett.* **B97**, 448 (1980).

29. Note that the $f_2'(1525)$ could, in principle, appear in $\pi^+\pi^-\pi^0\gamma\gamma$ via its decay to $\eta\eta$, where one $\eta \to \pi^+\pi^-\pi^0$ and the other $\eta \to \gamma\gamma$, with a net branching fraction of 0.026. This small branching ratio, combined with a tiny two-photon width (< 0.1 keV) [1], would make such a contribution undetectable in this experiment.

30. S. Godfrey and N. Isgur, *Phys. Rev.* **D32**, 189 (1985).

31. Indeed, our data in reference 6 show no evidence for $f_1(1510)$ in the reaction $\gamma\gamma^* \to KK\pi$, where the $f_1(1420)$ is prominently observed.

32. D. Bisello *et al.*, DM2 collaboration, *Phys. Rev.* **D39**, 701 (1989); R.M. Baltrusaitis *et al.*, Mark-III collaboration, *Phys. Rev.* **D33**, 1222 (1986).

33. T.A. Armstrong *et al.*, WA76 collaboration, *Phys. Lett.* **B228**, 536 (1989).

34. D. Alde *et al.*, GAMS collaboration, *Phys. Lett.* **B198**, 286 (1987).

35. H. Bienlein, Proceedings of Hadron'91, Maryland, Aug. 1991, ed. D. Peaslee (World Scientific, Teaneck, N.J., 1992).

Figure Captions

Figure 1 Invariant mass of $\gamma\gamma$ pairs from the single-tagged $\pi^+\pi^-\gamma\gamma\gamma$ sample (3 entries per event) for (a) all events, and (b) those events with an identified π^0. Note that the data in (b) were required to have a net transverse momentum (including tag) less than 0.25 GeV/c. The histogram in (b) represents a Monte Carlo simulation of the expected π^0 shape for two-photon production of $\pi^+\pi^-\pi^0\pi^0$ with a W-independent cross section and isotropic decay.

Figure 2 Transverse momentum squared of single-tagged (a) $\pi^+\pi^-\pi^0\gamma$ and (b) $\pi^+\pi^-\pi^0\pi^0$ data samples. Data are shown as points with error bars while the histograms are the results of the same Monte Carlo simulation used for Fig.1b. The arrows indicate subsequent cuts.

Figure 3 The detection efficiencies of the single-tagged $\pi^+\pi^-\pi^0\pi^0$ final state when one γ is undetected, as well as when the state is fully reconstructed, derived from a Monte Carlo model of spin-0 resonance production.

Figure 4 Invariant mass for the single-tagged $\pi^+\pi^-\pi^0\gamma$ events which pass all selection criteria.

Figure 5 Invariant mass for the untagged $\pi^+\pi^-\pi^0\gamma$ events which pass all selection criteria.

Figure 6 Invariant mass combinations from events in the region $1.25 \leq M\pi^+\pi^-\pi^0\gamma \leq 1.65$ GeV of the single-tagged $\pi^+\pi^-\pi^0\gamma$ final state.

Figure 7 Invariant mass combinations from events in the region $1.7 \leq M\pi^+\pi^-\pi^0\gamma \leq 2.2$ GeV of the single-tagged $\pi^+\pi^-\pi^0\gamma$ final state.

Figure 8 The peak $\pi^+\pi^-\pi^0\gamma$ invariant mass which would be observed as a function of the actual $\pi^+\pi^-\pi^0\pi^0$ invariant mass from a variety of Monte Carlo simulations described in the text. The solid diagonal line is the best linear fit to the points. The dashed horizontal lines represent peak masses of observed enhancements in the $\pi^+\pi^-\pi^0\gamma$ data spectrum, and the dotted lines give the mass uncertainty due to Monte Carlo model dependence.

Figure 9 Invariant mass of the single-tagged $\pi^+\pi^-\pi^0\gamma$ system, where the data from Fig.4 are plotted as points with error bars. The fit (histogram) includes Monte Carlo shapes for

resonance contributions as described in the text. The fit also includes a 3rd-order polynomial background shape which is shown separately as a solid curve. The dashed curve is an alternative background calculated from a fit to the untagged $\pi^+\pi^-\pi^0\gamma$ spectrum, under assumptions described in the text.

Figure 10 Invariant mass of the untagged $\pi^+\pi^-\pi^0\gamma$ system, where the data from Fig. 5 are shown as points with error bars. The histograms show the predictions for the R(1525) and R(2020) seen in single-tagged data, assuming they have spin-zero, added to a 4th-order polynomial fit to the untagged mass spectrum (solid curve).

Figure 11 The invariant mass of the single-tagged fully reconstructed $\pi^+\pi^-\pi^0\pi^0$ data sample. The data are shown as points with error bars, while the solid curve is a quadratic fit to the data. The solid histogram is the prediction of what should be seen in the $\pi^+\pi^-\pi^0\pi^0$ data, given the results for R(1525) and R(2020) from fits to the $\pi^+\pi^-\pi^0\gamma$ data, added to the quadratic background. The dashed curve is an alternative background calculated from a fit to the untagged $\pi^+\pi^-\pi^0\pi^0$ spectrum, under assumptions described in the text.

Figure 12 The invariant mass of the untagged fully reconstructed $\pi^+\pi^-\pi^0\pi^0$ data sample. The data are shown as points with error bars, while the histograms show the predictions for the R(1525) and R(2020) seen in single-tagged $\pi^+\pi^-\pi^0\gamma$, assuming they have spin zero, added to a 4th-order polynomial fit to the untagged $\pi^+\pi^-\pi^0\pi^0$spectrum (solid curve).

Figure 13 (a) The Q^2 evolution of the e^+e^- --> e^+e^-R(1525) cross section for Min($|q_1^2|$,$|q_2^2|$) < 0.1 GeV^2; (b) the two-photon coupling parameter times effective form factor, assuming the Cahn Model and $J_R = 1$, as a function of Q^2. The curves in (b) are predictions for the same quantity, using the measured value for the two-photon coupling parameter, with a ρ-pole form factor (solid curve) or a φ-pole form factor (dashed curve).

Figure 14 The invariant mass of the single-tagged $\pi^+\pi^-\pi^+\pi^-$ sample from reference 6. The smooth curve is the background shape used to calculate a conservative upper-limit on R(1525) and R(2020) production.

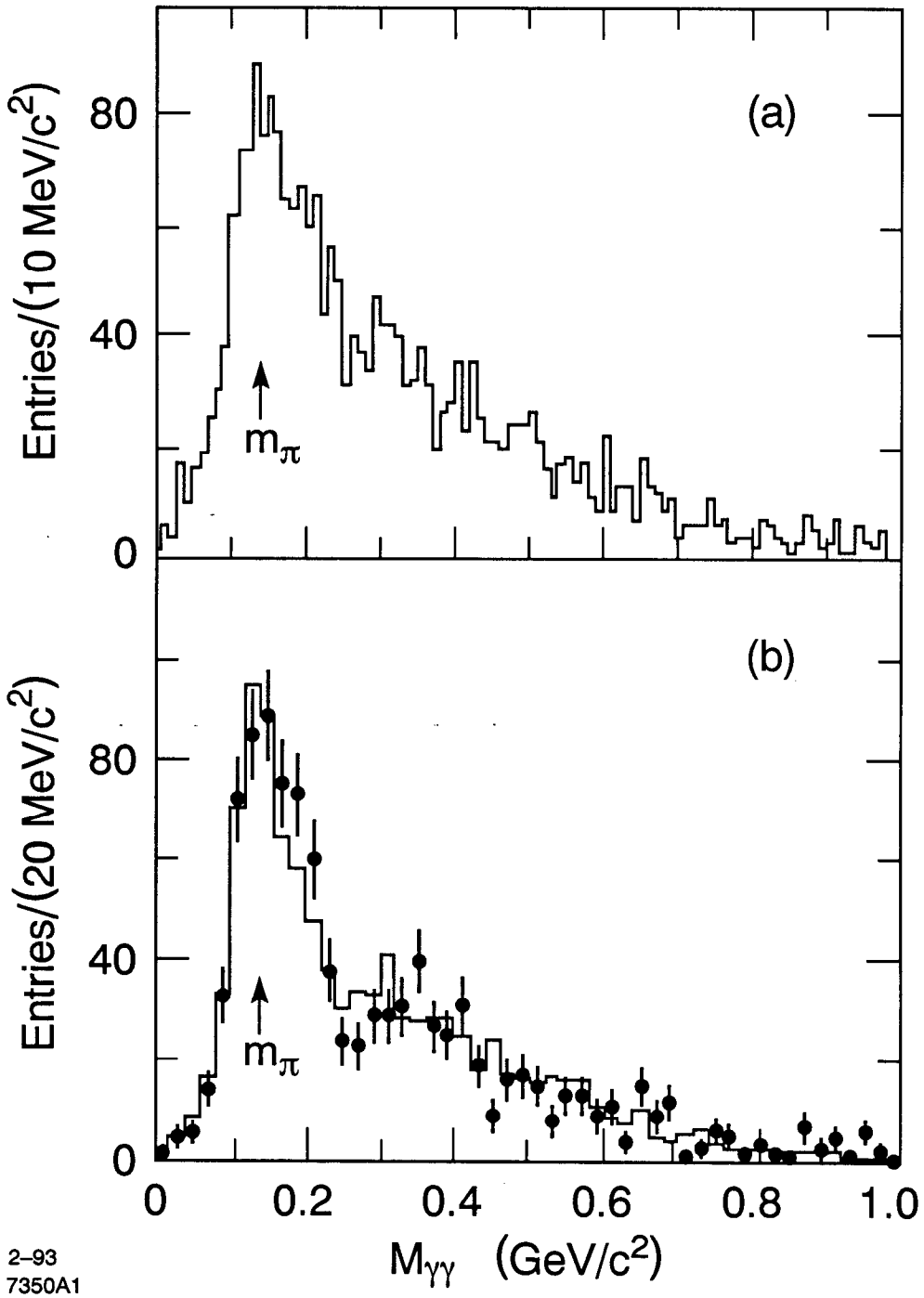
Entries/(10 MeV/c²)
80
40
0
(a)
mπ
Entries/(20 MeV/c²)
80
40
0
(b)
mπ
0
0.2
0.4
0.6
0.8
1.0
Mγγ (GeV/c²)
2–93
7350A1

Fig. 1

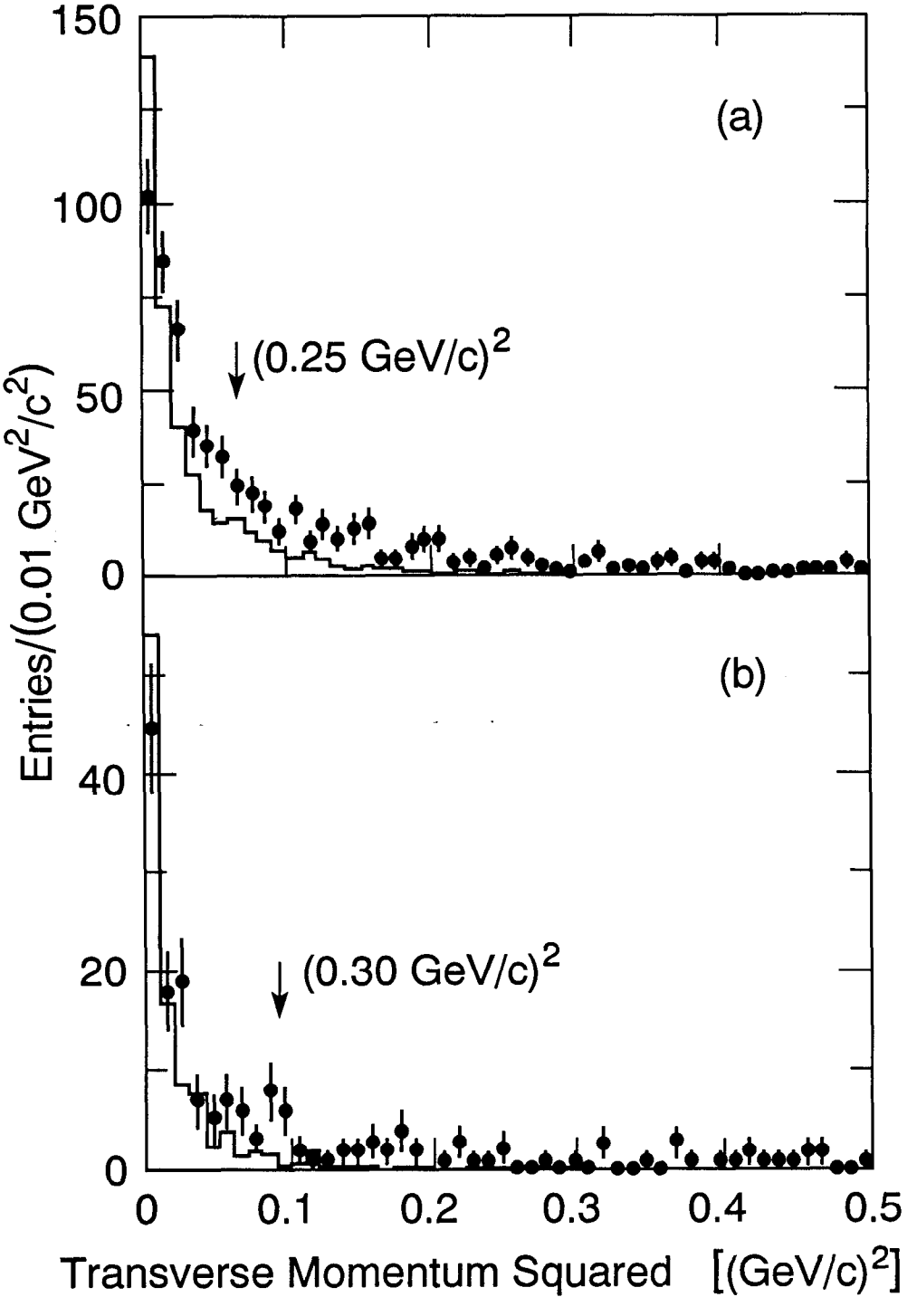
150
100
50
0
40
20
0
(a)
(b)
(0.25 GeV/c)^2
(0.30 GeV/c)^2
Entries/(0.01 GeV^2/c^2)
0
0.1
0.2
0.3
0.4
0.5
Transverse Momentum Squared [(GeV/c)^2]
2–93
7350A2

Fig. 2

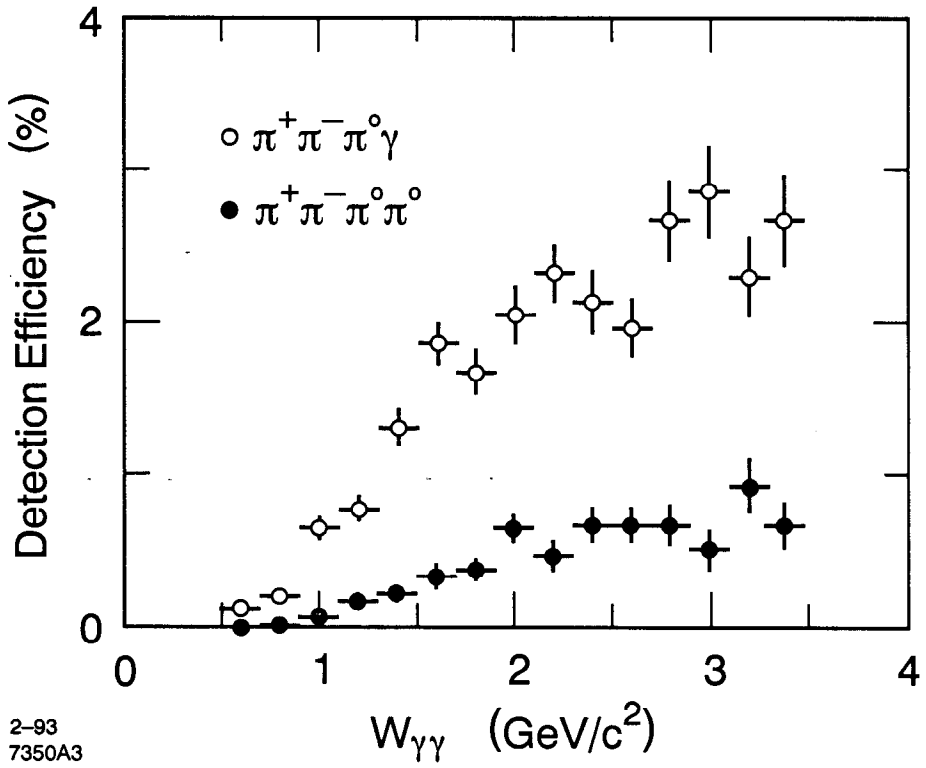
4
2
0
0
1
2
3
4
Detection Efficiency (%)
$\pi^+\pi^-\pi^\circ\gamma$
$\pi^+\pi^-\pi^\circ\pi^\circ$
$W_{\gamma\gamma}$ (GeV/c^2)
2–93
7350A3

Fig. 3

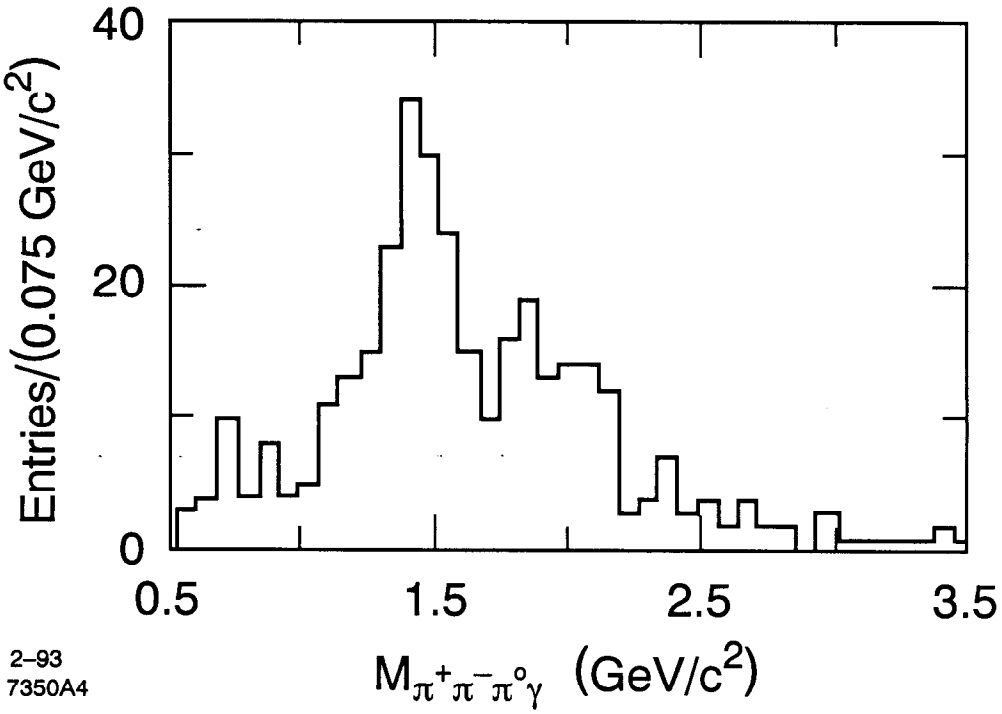

Fig. 4

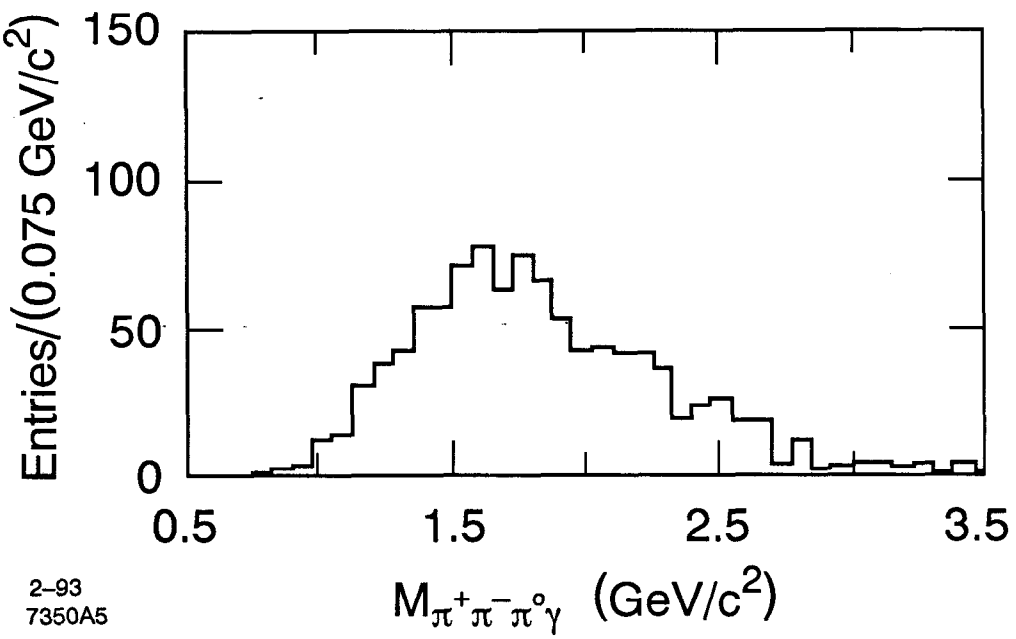
Entries/(0.075 GeV/c^2)
150
100
50
0
0.5
1.5
2.5
3.5
$M_{\pi^+\pi^-\pi^\circ\gamma}$ (GeV/c^2)
2-93
7350A5

Fig. 5

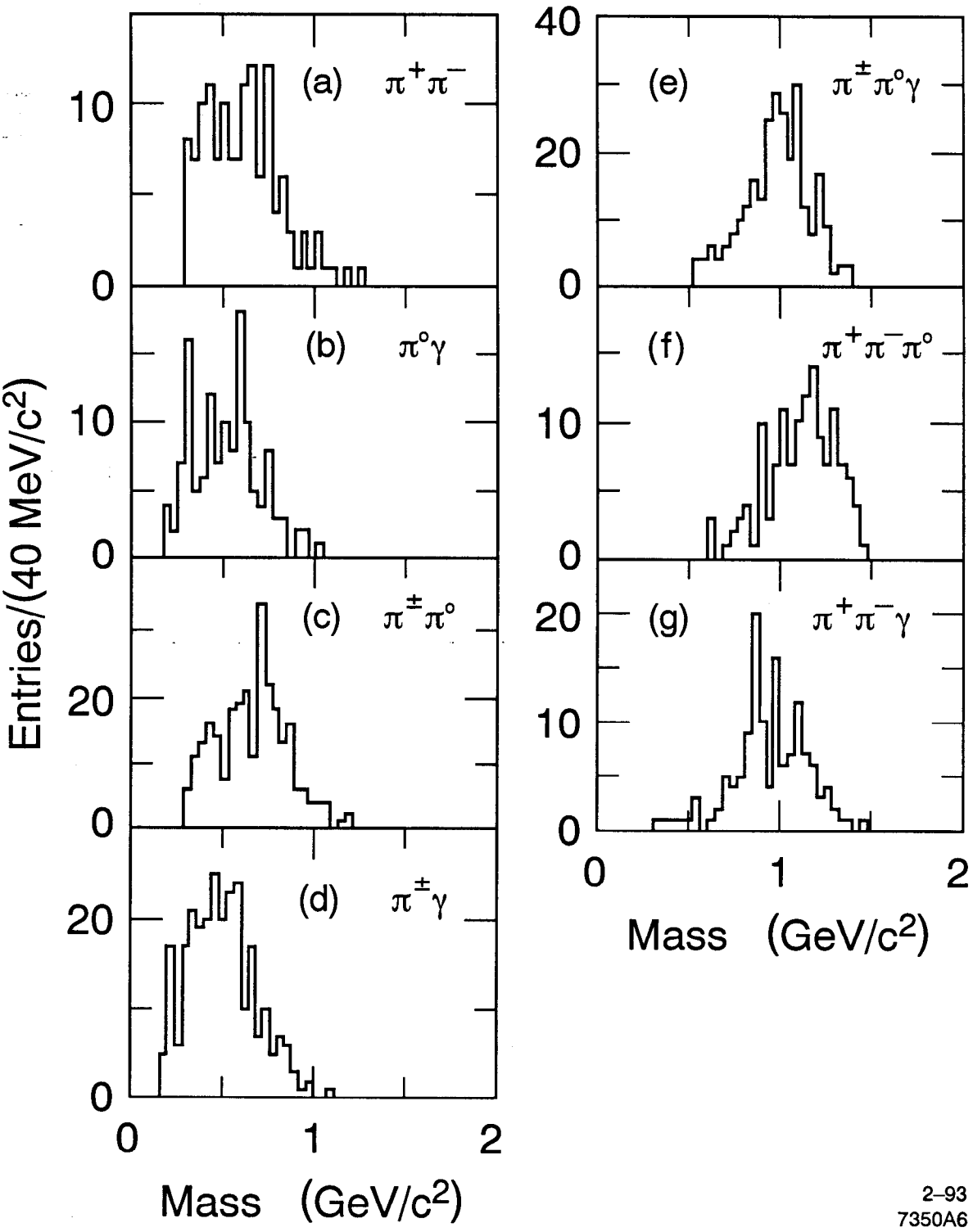
(a) $\pi^+\pi^-$
(b) $\pi^\circ\gamma$
(c) $\pi^\pm\pi^\circ$
(d) $\pi^\pm\gamma$
(e) $\pi^\pm\pi^\circ\gamma$
(f) $\pi^+\pi^-\pi^\circ$
(g) $\pi^+\pi^-\gamma$
Entries/(40 MeV/c^2)
Mass (GeV/c^2)
2–93
7350A6

Fig. 6

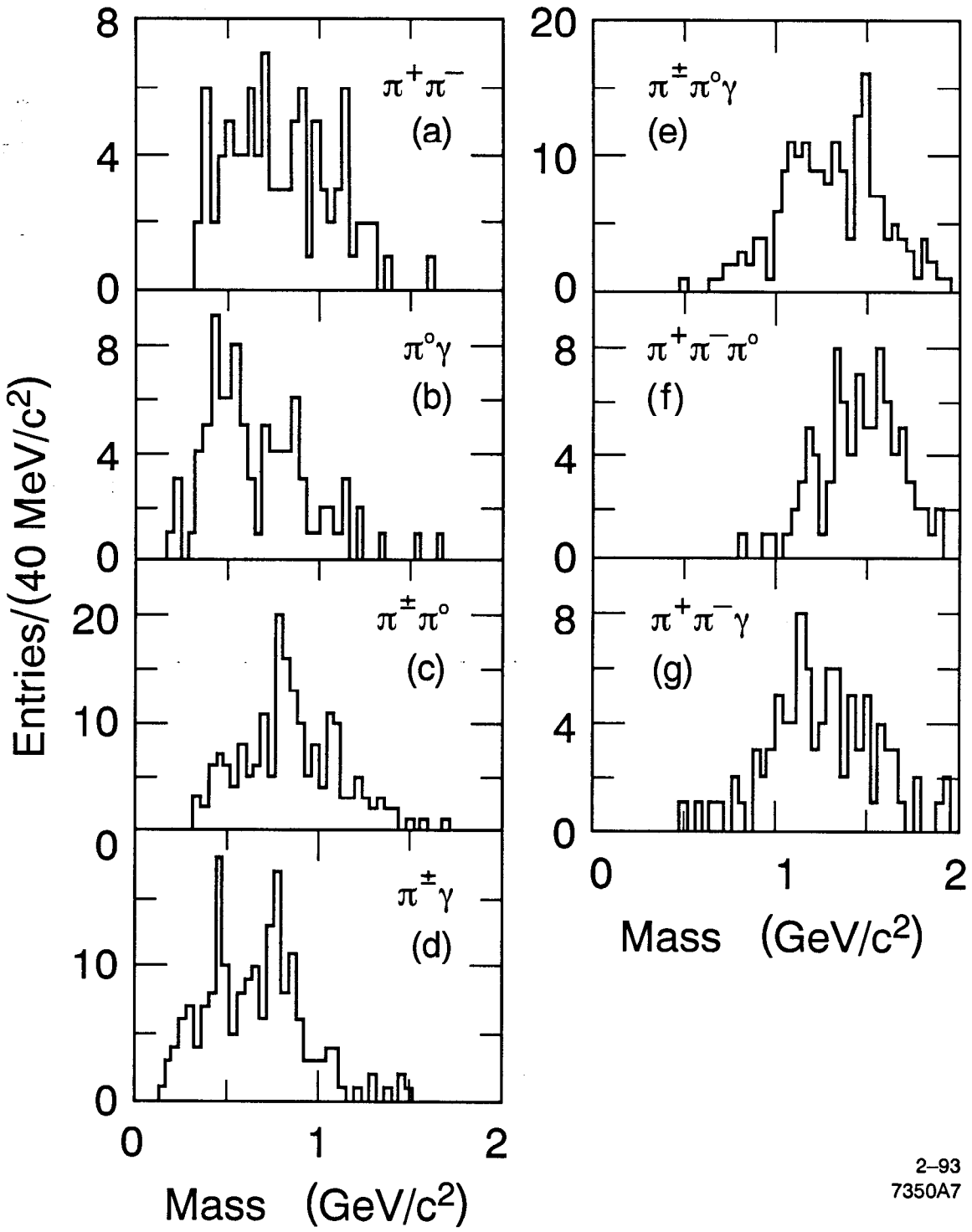
Entries/(40 MeV/c²)
π⁺π⁻
(a)
π°γ
(b)
π±π°
(c)
π±γ
(d)
π±π°γ
(e)
π⁺π⁻π°
(f)
π⁺π⁻γ
(g)
Mass (GeV/c²)
Mass (GeV/c²)
2–93
7350A7

Fig. 7

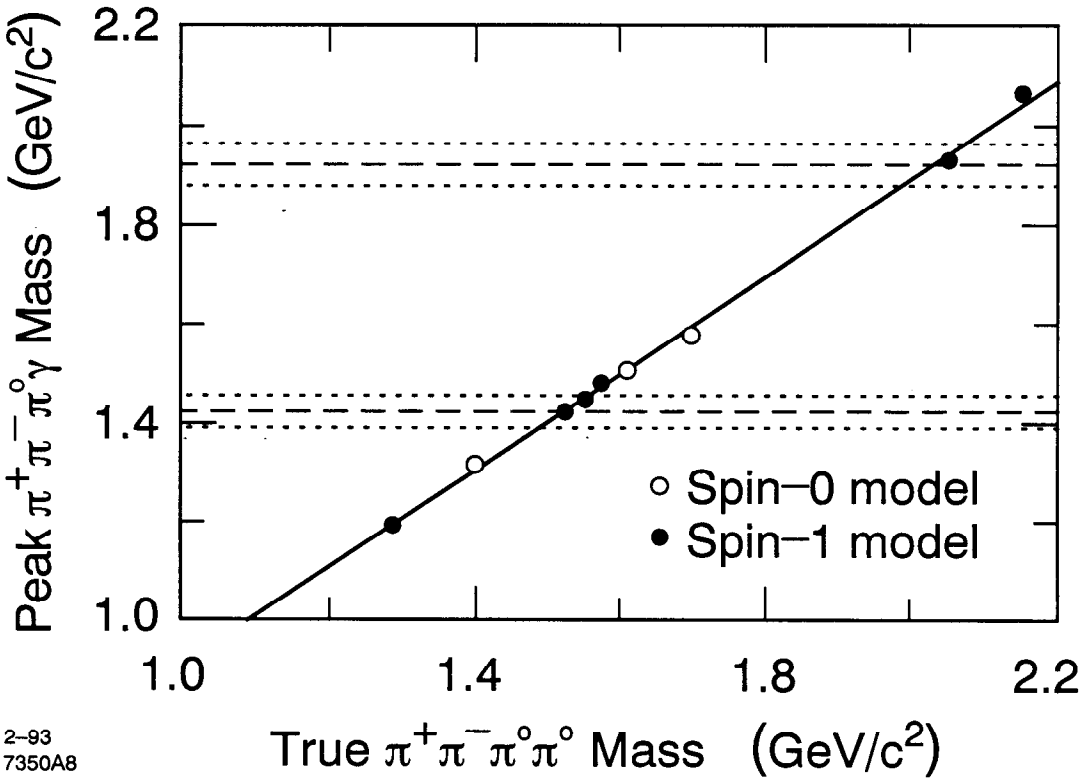
Peak $\pi^+\pi^-\pi^\circ\gamma$ Mass (GeV/c^2)
2.2
1.8
1.4
1.0
1.0
1.4
1.8
2.2
Spin–0 model
Spin–1 model
True $\pi^+\pi^-\pi^\circ\pi^\circ$ Mass (GeV/c^2)
2–93
7350A8

Fig. 8

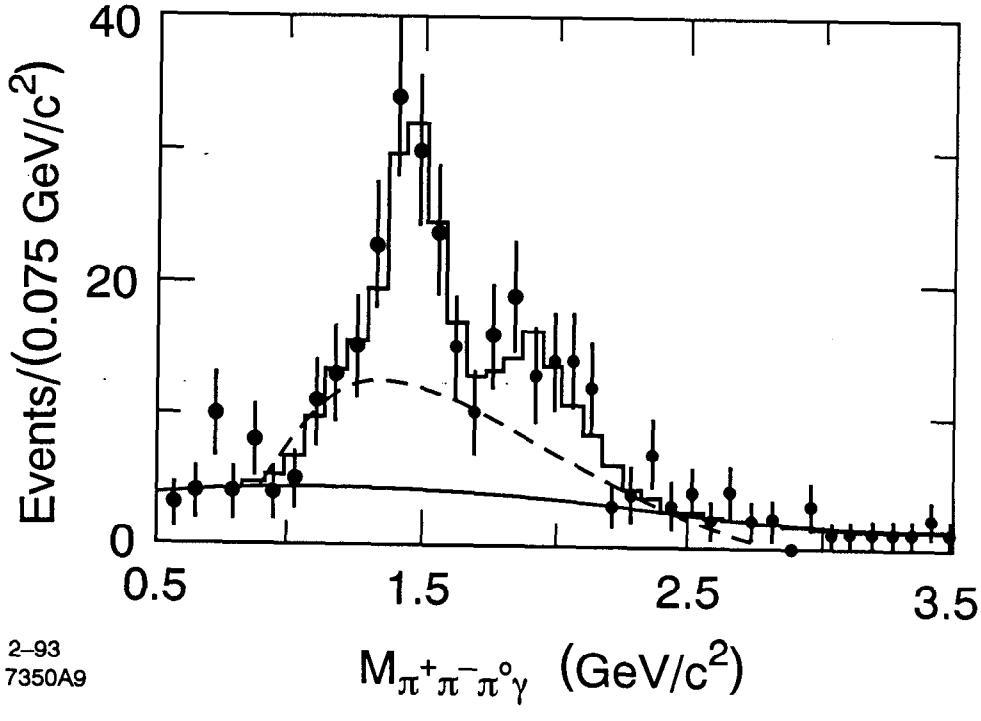

Fig. 9

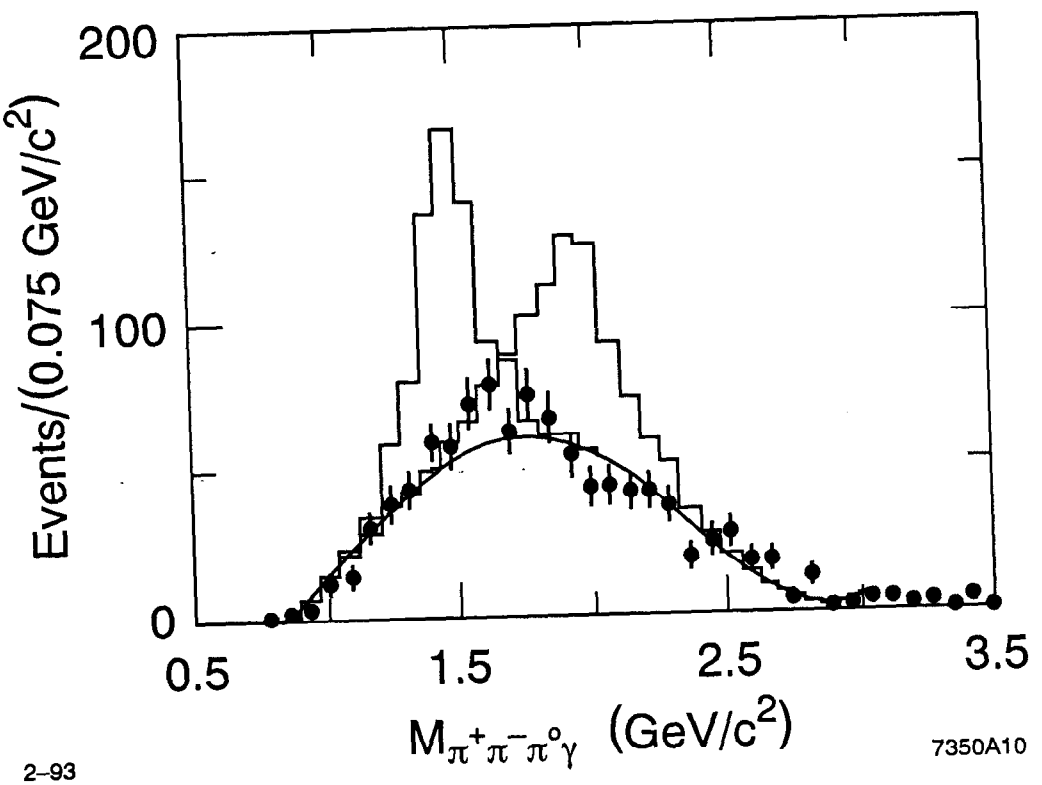
200
100
0
Events/(0.075 GeV/c^2)
0.5
1.5
2.5
3.5
$M_{\pi^+\pi^-\pi^0\gamma}$ (GeV/c^2)
2–93
7350A10

Fig. 10

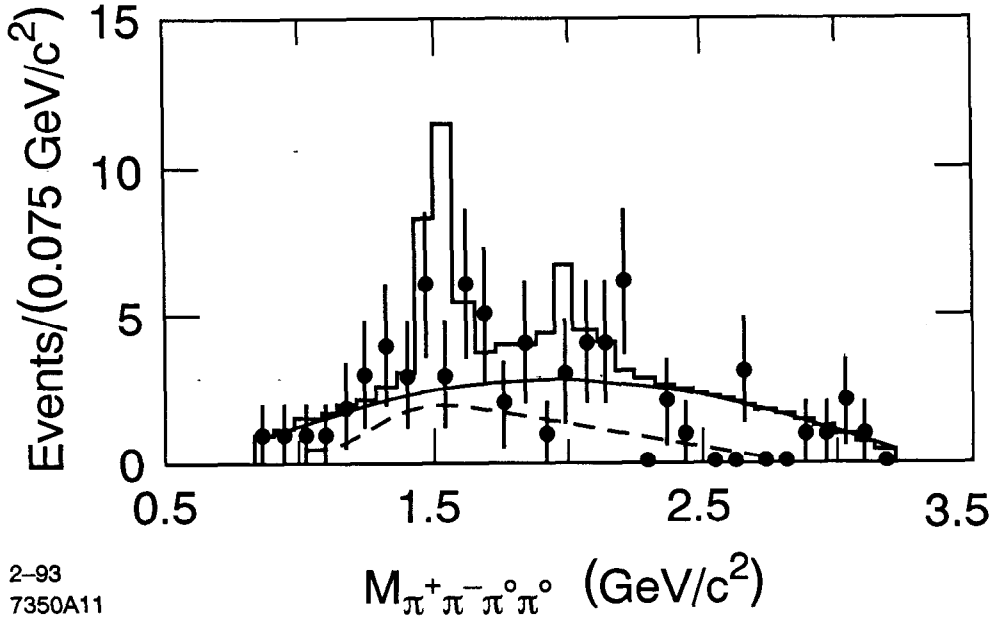

Fig. 11

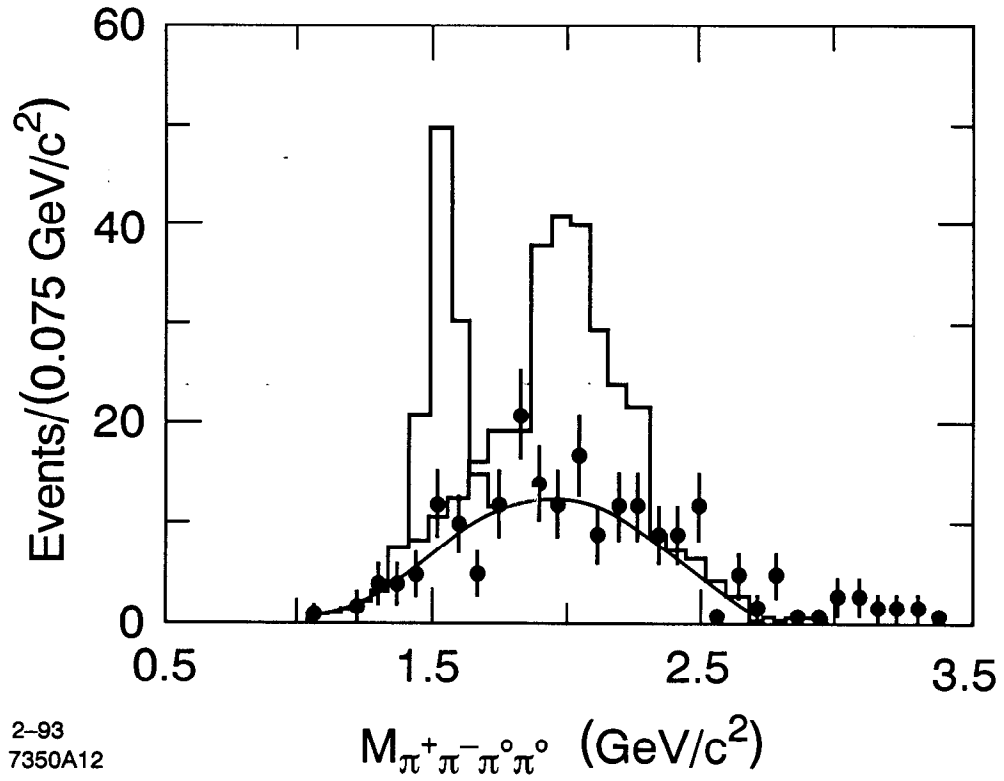
60
40
20
0
Events/(0.075 GeV/c²)
0.5
1.5
2.5
3.5
2–93
7350A12
Mπ⁺π⁻π°π° (GeV/c²)

Fig. 12

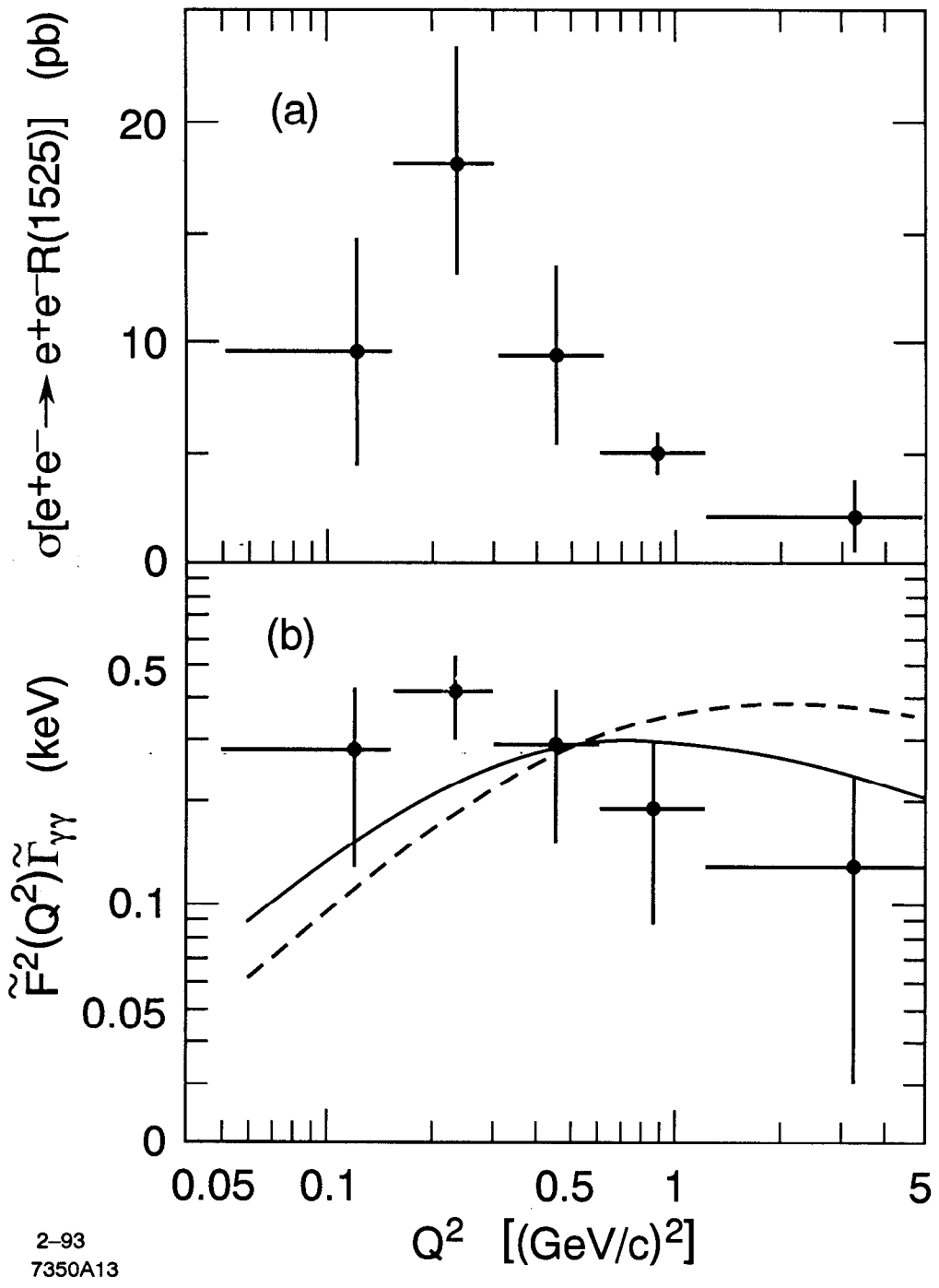
(a)
(b)
σ[e+e− → e+e−R(1525)] (pb)
F̃2(Q2)Γ̃γγ (keV)
Q2 [(GeV/c)2]
20
10
0
0.5
0.1
0.05
0
0.05
0.1
0.5
1
5
2–93
7350A13

Fig. 13

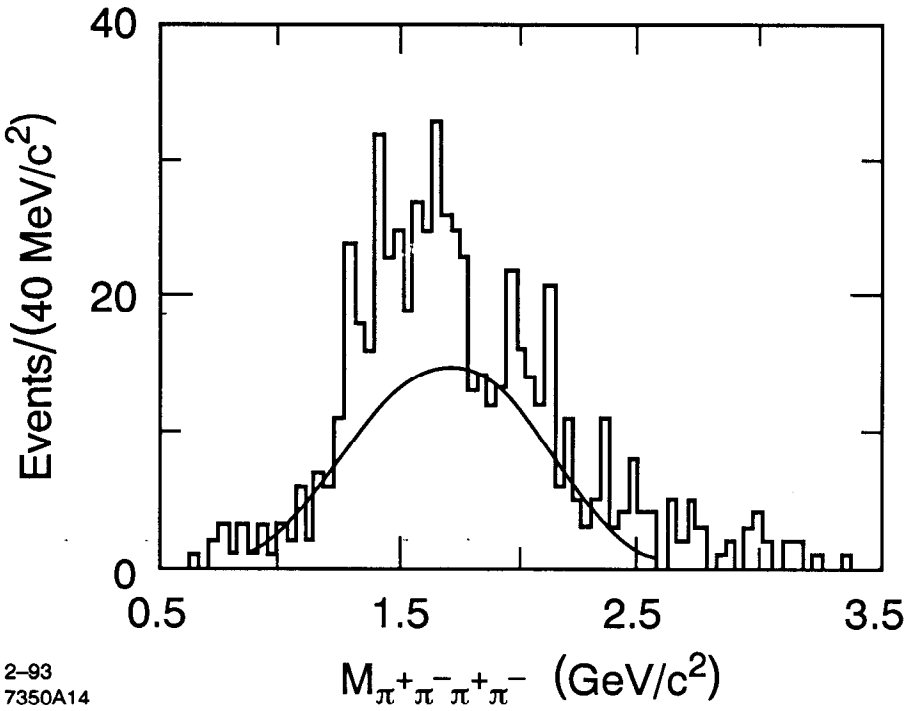

Fig. 14